

Abstract. We consider the evidence for very hard low energy spectra during the prompt phase of Gamma Ray Bursts (GRB). In particular we examine the spectral evolution of GRB 980306 together with the detailed analysis of some other bursts already presented in the literature (GRB 911118, GRB 910807, GRB 910927 and GRB 970111), and check for the significance of their hardness by applying different tests. These are among the bursts with the hardest low energy spectrum, sufficiently bright to allow time resolved spectral studies on time intervals of the order of tenths of a second. We discuss the hard spectra of these bursts and their evolution in the context of several non-thermal emission models, which all appear inadequate to account for these cases. The extremely hard spectra at the beginning of their prompt emission are also compared with a black body spectral model: the resulting fits are remarkably good, except for an excess at high energies (in several cases) which could be simply accounted for by the presence of a supra-thermal component. The findings on the possible thermal character of the evolving spectrum and the implications on the GRB physical scenario are considered in the frameworks of photospheric models for a fireball which is becoming optically thin, and of Compton drag models, in which the fireball boosts “ambient” seed photons by its own bulk motion. Both models appear to be qualitatively and quantitatively consistent with the found spectral characteristics.

Key words: gamma rays: bursts - methods: data analysis - radiation mechanisms: non-thermal.

Extremely hard GRB spectra prune down the forest of emission models

Giancarlo Ghirlanda¹, Annalisa Celotti¹, and Gabriele Ghisellini²

¹ SISSA/ISAS, via Beirut 2-4, I-34014 Trieste, Italy;

² Osservatorio Astronomico di Brera, via Bianchi 46, I-23807 Merate, Italy.

1. Introduction

Since the discovery of these mysterious and puzzling cosmic explosions, the time resolved spectral analysis of Gamma Ray Bursts (GRBs) have been a testing ground-floor for the models proposed for the γ -ray prompt emission (Ford et al. 1995, Crider et al. 1997). In particular, different authors (Crider et al. 1997, Preece et al. 1998) have stressed the importance of studying the low energy component of GRB spectra which is one of the better determined and accessible observables. In general GRBs have a continuous curvature spectrum which is usually characterized (Band et al. 1993) by two smoothly joining components defining a peak (in a EF_E representation) around 200 keV. The low energy part can be modeled as a power law function in the photon distribution $N(E) \propto E^\alpha$ (i.e. $EF_E \propto E^{\alpha+2}$). The high energy spectral component can be described in most cases by a steep power law E^β (with $\beta < \alpha$) or an exponential cutoff. The typical values of α and β are widely distributed around -1 and -2.5 respectively (Preece et al. 2000; see also Fig. 1).

The most popular emission model proposed for interpreting such γ -ray spectra is synchrotron emission by relativistic electrons in intense magnetic fields (Rees & Meszaros 1994; Katz 1994; Tavani 1996), but alternative scenarios have been proposed, such as Comptonization of low energy photons by thermal or quasi-thermal particles (Liang et al. 1997; Ghisellini & Celotti 1999). The physical parameters of these models can be tuned and combined to justify the principal observed temporal and spectral characteristics of GRBs, producing a considerable number of plausible spectral shapes. Furthermore, more complex variants on these basic emission processes have also been postulated, such as jitter radiation (Medvedev 2001), synchrotron emission from particles with an anisotropic pitch angle distribution (Lloyd & Petrosian 2000, 2002); thin/thick synchrotron emission from a stratified region (Granot, Piran & Sari 2000); synchrotron self-Compton or inverse Compton off photospheric photons (Meszaros & Rees 2000); Compton drag (Lazzati et al. 2000; Ghisellini et al. 2000). Although the variety of the proposed models (or combination of models) corresponds to a variety of predicted spectra, the most extreme (in this case hardest) low energy observed spectra and their evolu-

Table 1. Low energy limiting photon spectral indices α [i.e. $N(E) \propto E^\alpha$] for various emission models. For clarity the indices in flux $F(E)$ and $EF(E)$ representation are also reported.

α $N(E)$	$\alpha + 1$ $F(E)$	$\alpha + 2$ $EF(E)$	model
-3/2	-1/2	1/2	Synch. + cooling
-1	0	1	Quasi-saturated Comptonization
-2/3	1/3	4/3	Synch. instantaneous
0	1	2	Small pitch angle/jitter/IC single e^-
1	2	3	Black Body
2	3	4	Wien

tion can be used to rule out or constrain some of the possibilities.

To the aim of testing the validity/generality of the proposed models we have then searched in the published spectral catalog of Preece et al. (2000) for the hardest low energy component spectra and found two extremely hard bursts: GRB 911118 (whose peak energy evolution has been reported in Ford et al. 1995 spectral catalog) and a new case, GRB 980306. These two GRBs are carefully studied here in terms of their low energy spectral hardness and especially their spectral evolution on timescales of few tenths of a second (Sec. 4.1, 4.2), together with other hard bursts reported by Crider et al. (1997, 1997, 2000) and Frontera et al. (2000): GRB 910807, GRB 910927 and GRB 970111 (Sec. 4.4). We also present the tests that we performed in order to determine the statistical robustness of the spectral hardness, and in particular a model independent approach consisting in the comparison of each spectrum with a template one of given hardness (Sec. 4.3). The evidence that, at least at the beginning of the bursts, the spectra could have a black body character is discussed in Sec. 4.5. The comparison with the low energy spectral limits predicted by different models (briefly recalled in Sec. 2 together with the previous evidence of hard spectra) is the content of the discussion (Sec. 5) where also tentative interpretations of the initial quasi-thermal spectral evolution, in the context of the hot fireball model and in the Compton drag model, are presented. We draw our conclusions in Sec. 6.

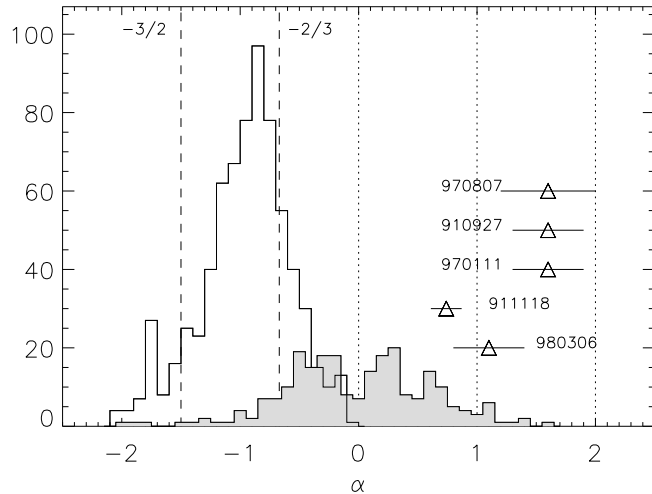


Fig. 1. Low energy spectral index distribution from Ghirlanda, Celotti & Ghisellini (2002). The vertical lines represent the limits of the emission models reported in Tab. 1 and plotted in Fig. 2. The triangles represent the maximum values found from the spectral analysis of the bursts presented in this work along with their 90% confidence interval (horizontal bars). The grey histogram shows the distribution of the low energy spectral index found from the time resolved spectral analysis of the bursts presented in this work. The triangles represent the maximum α values for the same bursts.

2. Spectral Slopes and Emission Models

The distribution of the low energy photon spectral index α obtained from the time resolved spectral analysis of a sample of bright BATSE bursts (Ghirlanda, Celotti & Ghisellini 2002) is reported in Fig. 1. The majority of GRB spectra (Preece et al. 2000, Ghirlanda et al. 2002) have a low energy power law spectral index $-3/2 < \alpha < -2/3$, i.e. within the limits predicted by the optically thin synchrotron model (Fig. 2, dashed lines; see also Katz 1994), but there is a non negligible fraction of bursts ($\sim 15\%$, see also Preece et al. 2000) showing a slope harder than $\alpha = -2/3$. The spectral analysis of a sample of GRBs by Crider et al. (1997) revealed that the spectrum, integrated over the pulse rise phase, is harder than $E^{-2/3}$ for the 40% of their bursts and can be as hard as $N(E) \propto E^1$ (i.e. $EF_E \propto E^3$). For comparison the hard spectra of the bursts considered in this paper are also reported (grey histogram) in Fig. 1, showing that they contribute to extend the distribution toward positive α values up to ~ 1.5 .

Let us here just recall that this evidence is hardly reconcilable with the simplest formulation of the synchrotron model and some alternatives have been proposed to account for these observations within the frame of this emission process (Papathanassiou 1999, Granot, Piran & Sari 2000). Lloyd & Petrosian (2000) propose a scenario in which electrons have a small pitch angle distribution (SPD in Fig. 2), extending the range of possible low energy spectral indices produced via synchrotron to the limit $\alpha \sim 0$. The same limiting slope can be ob-

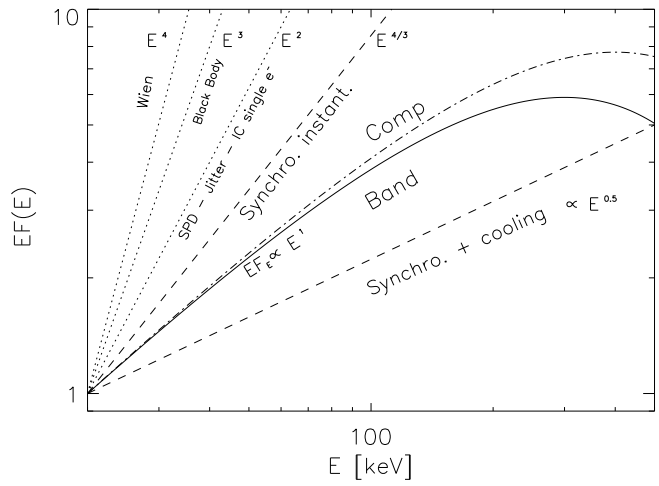


Fig. 2. Low energy spectral component. Example of the BAND (solid line) and COMP model (dot-dashed line) with the low energy photon spectral index fixed at -1 [i.e. $EF(E) \propto E^1$]. For comparison we report the spectral slopes predicted by the emission processes reported in Tab. 1.

tained in the “jitter” radiation theory, which results from synchrotron emission in a non uniform magnetic field with inhomogeneities on length scales smaller than the electron gyroradius (Medvedev 2001). Slopes even harder (i.e. $\alpha \sim 1$) may instead correspond to thermal radiation, such as a portion of a black body spectrum or saturated Comptonization spectra with Wien peaks which can be as hard as $\alpha \sim 2$ (Liang et al. 1997, Ghisellini & Celotti 1999, Ghisellini et al. 2000).

A detailed discussion of these models and their comparison with our observational findings are presented in Sect. 6. As reference for the following sections here we schematically summarise the model predictions in Tab. 1, and display in Fig. 2 their typical low energy limiting slopes in $EF(E)$.

3. Data Analysis

We have analysed the Large Area Detector (LAD) High Energy Resolution Burst (HERB) data which have a high count rate, due to the LAD large effective area, and are suited for the spectral analysis of GRBs for which a moderate energy resolution is sufficient to study the typical GRB broad band continuum (Preece et al. 1998).

We selected the data from the most illuminated detector which has the highest S/N, and maintained the instrumental time binning corresponding (in the best cases) to single time resolved spectra accumulated for 128 ms, to follow the spectral variations on the smallest possible timescale. Each spectrum has been fitted from $E_{\min} \sim 28$ keV to $E_{\max} \sim 1800$ keV which define the typical energy window for the LAD data (Preece et al. 1998, 2000). An individual energy rebinning scheme has been systematically applied to reach a level of 30 counts per channel to be confident that the Poisson statistics is

represented by a normal distribution (for the validity of the χ^2 test).

The spectral analysis has been carried out using SOAR (1993) as a quick look tool for the spectral evolution and then XSPEC for the individual spectral fitting of time resolved spectra. The background spectrum, to be subtracted to each time resolved spectrum, has been calculated as the average over a selected number of background spectra accumulated before and after the trigger.

3.1. Fitting models

We fitted the most commonly adopted GRB spectral models: the BAND (Band et al. 1993) and COMP model, represented by a smoothly connected double power law or by a single power law ending with an exponential cutoff, and the sharply connected double power law model (BPLW). The choice of these models is motivated by the fact that they characterise the low energy part of the spectrum with a spectral parameter (i.e. the spectral index α) which can be simply compared with the predictions of different radiative models. For a detailed description of these spectral functions see Preece et al. (2000).

Due to the extreme hardness of the low energy spectrum of these bursts, we decided also to verify if thermal, black body like, emission was consistent with the low energy data. This was done on the hardest spectra, selected for having a spectral index harder than $\alpha = 0.5$ from the BAND/COMP models. This indicative value, which is softer than $\alpha = 1$ (i.e. the Rayleigh-Jeans limit of a black body spectrum) has been chosen to: a) account for typical errors in the determination of α with the BAND or COMP models; b) include the possibility that the spectrum could be softer than $\alpha = 1$, if its peak is at low energies (due to the spectral curvature).

The result of each fit was then considered acceptable if the reduced χ^2 was lower than 1.5: in fact the statistical probability of having a better fit is around 0.5 if the reduced χ^2 is around 1, but a limiting value of $\chi^2_{\text{red}} \sim 1.5$ is suggested if one considers that χ^2_{red} depends on the quality of the data (Bevington & Robinson 1992). In addition we visually inspected the data-to-model ratio to look for possible systematics (i.e., sequence of points significantly above or below unity). We discarded the black body as a good fit when an excess of flux occurred at low energies (i.e. in the E^2 part of the spectrum), while we allowed for (a moderate) deviation from unity at high energies (i.e. in the exponential part). This latter choice reflects the possible (or even likely) situation of having a “supra-thermal” tail to a Maxwellian distribution in quasi-thermal plasmas, or it could be produced by a multi-temperature black body emission.

4. Results

Sec. 4.1 deals with the new case of hard low energy burst: GRB 980306. In particular we focus on the early phase of this burst when the spectrum is extremely hard. The detailed spectral evolution analysis of GRB 911118 (Ford et al. 1995) is reported in Sec. 4.2 with emphasis (again) on the low energy spectral in-

dex evolution. In Sec. 4.3 we describe the tests we performed on the raw data to check for the significance of the found spectral hardness of these two bursts. In Sec. 4.4 we briefly discuss other 3 bursts (GRB 910807, GRB 910927 and GRB 970111) with hard spectra that we have found through a search in the literature and that we have reanalyzed, applying the tests described in Sec. 4.3, to verify their low energy hardness. In particular for GRB 910807 we have extended the time analysis beyond the first 5 seconds that were previously studied by Ryde & Svensson (1999). The results relative to the black body fits are separately reported in Sec. 4.5.

4.1. GRB 980306

GRB 980306 (BATSE trigger 6630) represents a newly discovered case of hard burst. It is a single peak FRED-like burst (Fig. 3, *top panel*) with duration of ~ 6 s, peak flux of (17.2 ± 0.4) phot $\text{cm}^{-2} \text{s}^{-1}$ at $t_{\text{peak}} \sim 2.2$ s and a total (100–300) keV fluence of $\sim 10^{-5}$ erg cm^{-2} . This burst was already present in Preece et al. (2000) spectral catalogue but, as it had been fitted with a BPLW model only, it did not reveal its hard low energy component. In fact, as already noticed in Ghirlanda et al. (2002), a fit of a model with a sharp break, like the BPLW, to a smoothly curved spectrum, although can still give acceptable fits, tends to underestimate the low energy spectral hardness.

We present, for the first time, its hardness evolution, and more precisely the spectral evolution of the first 6 s, divided in 14 time resolved spectra. The spectral fits with the different models show that the spectra are better represented by the COMP model, since the high energy spectrum are very steep (i.e. steeper than a power law with spectral index $\beta = 10$, the limit of the fitting function). The best fit parameters for this model are plotted in Fig. 3 (mid and bottom panels) as a function of time.

The hardness evolution of the burst is typically described by how the spectral index α and $E_{\text{peak}} = (\alpha + 2)E_0$ change in time (here E_{peak} is the peak energy and E_0 the exponential cut-off characteristic energy). For this specific burst the evolution is hard-to-soft, as shown by the peak energy (bottom panel of Fig. 3) decreasing in time from ~ 150 keV to ~ 50 keV at the end of the burst. The evolution of α (mid panel of Fig. 3) indicates that, in the rising phase of the pulse, there is a trend toward hardening, with the maximum hardness ($\alpha = 1.1 \pm 0.2$) reached at $t_{\text{mh}} \sim 1.5$ s (although in the first seconds of the burst α is also consistent with being constant). After t_{mh} the spectrum softens, but it remains harder than $\alpha = 0$. We stress that the low energy spectrum is significantly (more than 3σ) harder than $\alpha = 0$ for each of the first 7 time resolved spectra (between $t = 0$ and $t = 2.24$ s).

In view of the discussion on the spectral models (Sect. 6) we also checked the inadequacy of the optically thin synchrotron model by fitting the BAND spectrum with the low energy power law slope fixed at $-2/3$. As expected, the residuals at low energies show a systematic sign and indicate that the model is not a good representation of the data.

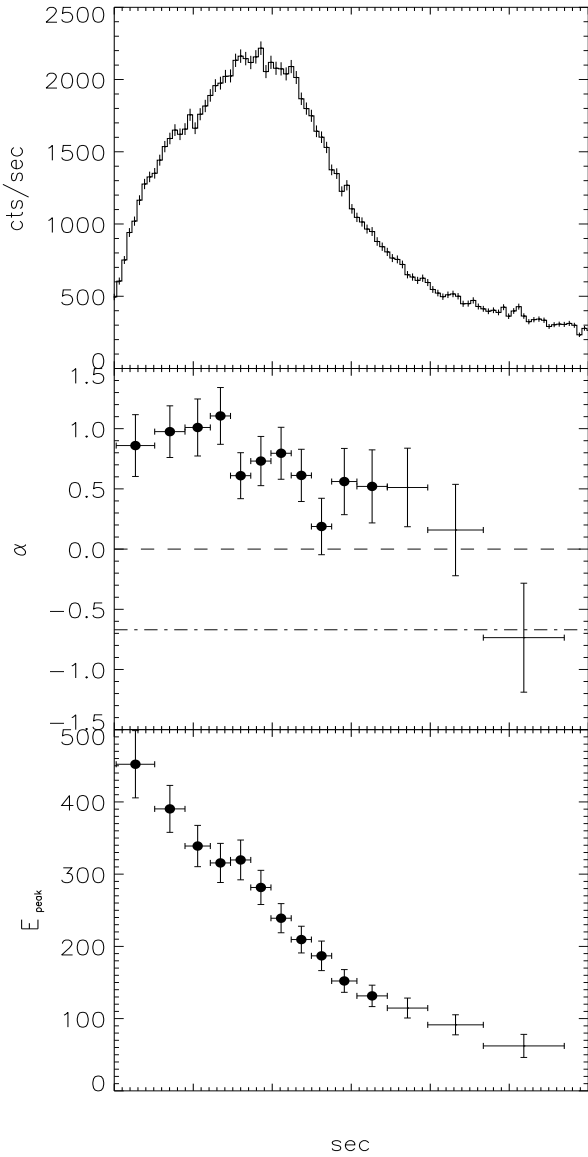


Fig. 3. Light curve and best fit parameters for GRB 980306. Top panel: light curve on the 64 ms timescale, integrated in the range 110–320 keV. Mid panel: low energy power law spectral index (α). Horizontal lines mark the limits $\alpha = -2/3$ and $\alpha = 0$. Bottom panel: peak energy E_{peak} of the $EF(E)$ spectrum. Error bars represent the 90% confidence interval on the best fit parameters. The filled circles indicate the spectra which have been fitted also with a blackbody model (see Tab. 2 and Sec. 4.5)

4.2. GRB 911118

The light curve of GRB 911118 (BATSE trigger 1085), reported in Fig. 4 (*top panel*), has two main peaks which partially overlap. It is a typical long burst with total duration $T_{90} = 19.2 \pm 0.1$ s and a background subtracted peak flux of (30.6 ± 0.8) phot $\text{cm}^{-2} \text{ s}^{-1}$ at $t_{\text{peak}} = 6.08$ s. Its fluence,

in the 100–300 keV energy range, is $(27.8 \pm 0.1) \times 10^{-6}$ erg cm^{-2} .¹

The spectral analysis that we present is limited to the first 13 s after the trigger time (for a total of ~ 50 spectra), in which the time resolved spectrum evolves dramatically with an excursion of $\Delta\alpha \sim 1$ and $\Delta E_{\text{peak}} \sim 400$ keV. The best fit is obtained with the BAND model. The low energy spectral index is $\alpha > 0$ for the first ~ 6 s (32 spectra, phase A of Fig. 4, mid panel) and decreases with time (the spectrum softens), but remains harder than $-2/3$ for the time interval up to the end of phase B. After $t \sim 13$ s, the spectrum has a typical $\alpha < -2/3$ slope. The hardest spectrum (at $t \sim 1.5$ s after the trigger) has $\alpha = 0.74 \pm 0.13$ corresponding to $EF_E \propto E^{2.74 \pm 0.3}$. The significance of a positive value of α for the spectra of phase A is high, being $> 3\sigma$ for most of the individual spectra (23/32). The peak energy evolution reported in Fig. 4 (bottom panel) is consistent with what reported by Ford et al. (1995) and Crider & Liang (1999). According to these fits, the 18 spectra belonging to phase B have $-2/3 < \alpha < 0$ and their evolution is of the “hard-to-soft” kind, i.e. the peak energy decreases in time (becoming smaller than 200 keV in phase B). From Fig. 4 it can be seen that there is a correlation between the peak energy E_{peak} and α .

Again we also tried to fit the simplest optically thin synchrotron model (by fixing the low energy spectral index of the BAND model to $-2/3$). In Fig. 5 we report, for comparison, the values of the reduced χ^2_r for all spectra. The best fit is given by the BAND model (asterisks) while the “synchrotron” (triangles) is inadequate to fit these spectra. The value of χ^2_r for the synchrotron model becomes marginally acceptable for some spectra in phase B.

We conclude that the time resolved spectra of this burst are best represented by the BAND model with the 4 fit parameters free to vary and that most of the spectra of phase A have $\alpha > 0$ at a 3σ level.

4.3. Tests on the Spectral Results

Considering the relevance of the extreme hardness of these bursts for the comparison with the models, we performed different checks to verify if and at what confidence level they can be considered harder than the predictions of the proposed spectral models (as in Tab. 1). In the following we report on the tests performed on the above burst spectra and their results.

– *reduced fitting energy range*: we eliminated from the fitting energy range the high energy channels to test if they substantially influence the low energy fitted spectral slope. We restricted the analysis to the range 28–600 keV (the upper limit being the maximum peak energy found among the bursts presented) and compared the results with those obtained by fitting the spectra on the entire energy window (i.e. up to 1800 keV). We found that the best fit spectral parameters are consistent within their errors and α from the limited energy range case is still inconsistent with $\alpha = 0$;

¹ <http://cossc.gsfc.nasa.gov/batse/4Bcatalog/index.html>

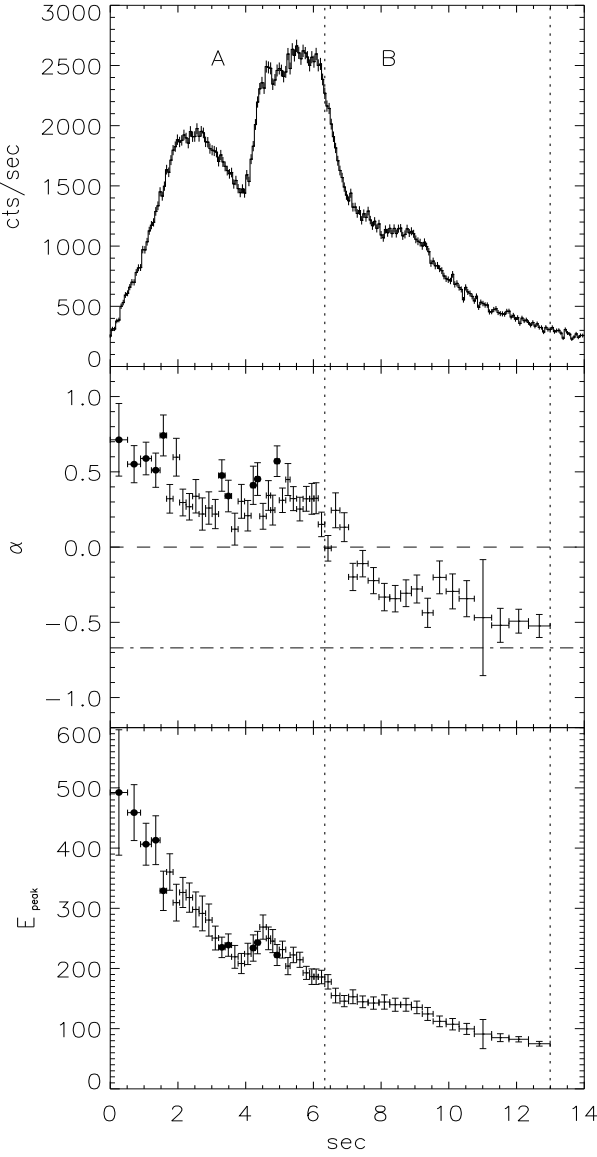


Fig. 4. The light curve and time evolution of the spectrum fitted with the BAND model for GRB 911118. Top panel: light curve on the 64 ms timescale in the energy range 100 – 320 keV, summed over all the triggered detectors. The vertical dotted lines represent the boundaries of the phases in which the spectrum is harder than E^0 (phase A) and $E^{-2/3}$ (phase B). Mid panel: low energy power law spectral index α , with the limits at $\alpha = -2/3$ (dot-dashed) and $\alpha = 0$ (dashed). Bottom panel: Peak energy of the $E_{\text{F}}E$ spectrum. The filled circles represent the spectra which have been fitted also with a blackbody model (see Tab 2 and Sec. 4.5).

– *background spectrum*: if the background spectrum were characterised by any feature or absorption edge at low energies (e.g. dependent on some electronic failure or anomalous observational conditions) this might determine particularly hard low energy power laws in the background sub-

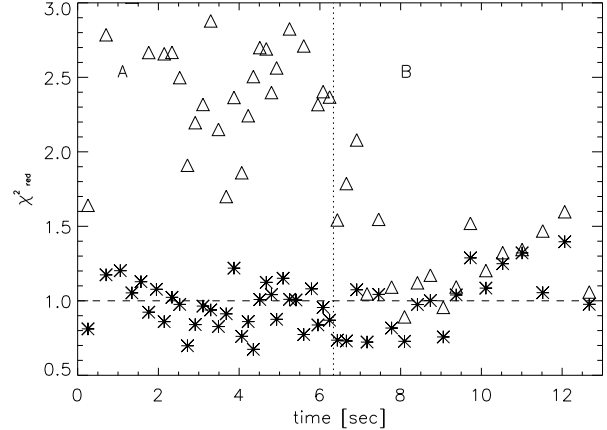


Fig. 5. Reduced χ^2 of the fits with different models to the spectra of GRB 911118: BAND model (asterisks), BAND model with the low energy spectral index fixed at $-2/3$ (triangles).

tracted spectra. In order to exclude this possibility we computed several backgrounds selecting different time intervals, within the same GRB and found that the background spectrum does not depend on the time interval selected for its calculation. Moreover, we also fitted the spectra adopting different backgrounds calculated for other bursts: the results indicate that α is not affected by anomalous features in the background spectrum.

– *detector response*: the detector response matrix, if incorrectly calculated, could determine a wrong set of best fit parameters. We believe this is unlikely as, by fitting the spectra with the detector response matrix (DRM) associated with another burst but for the same LAD, the results are consistent within their 90% confidence level;

– *comparison with a simulated spectrum*: the most direct and robust way to verify if the deconvolved spectra are really as hard as we found is to compare them with a reference spectrum whose shape is well defined. For every time resolved spectrum that we analysed, we thus simulated a reference (template) spectrum with a low energy power law slope $\alpha \sim 0$ and a break energy fixed at the value obtained from the fit of the observed spectrum. We divided channel by channel the observed spectrum by the template and then analysed the ratio (as long as the observed spectrum is harder than the template one their ratio at low energies increases with energy). In order to quantify the hardness we fitted such ratio with a power law. The fitted index δ is reported in Fig. 6 and 7 for GRB 911118 and GRB 980306, respectively. We note that during phase A (the first 6 s after the trigger) of GRB 911118 each of the time resolved spectra is at least 3σ harder than a flat spectrum (i.e. with the same level of confidence that was found with the direct fitting method). In the case of GRB 980306 this test gives a fitted ratio with a poor level of confidence ($< 2\sigma$) for each spectrum (with only two spectra at $> 2\sigma$) because of the lower S/N due to count statistics and due to the propagation

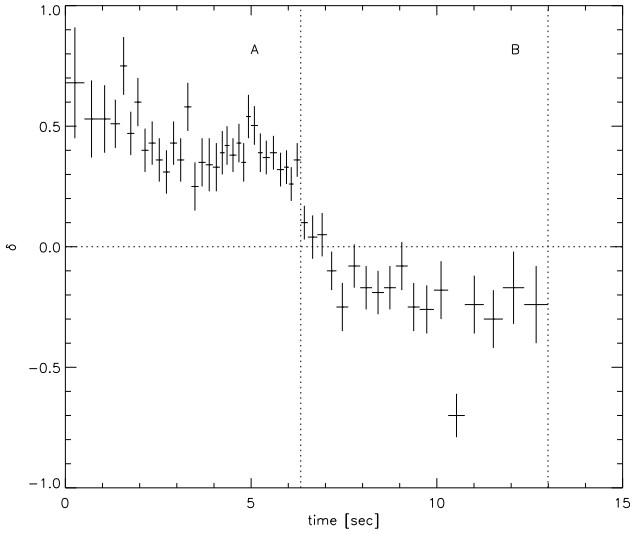


Fig. 6. GRB 911118 - Slope of the power law fitted to the ratio between the observed time resolved spectra and the template spectra (simulated with $\alpha = 0$ and $E_{break} = E_0(fit)$). Labels A and B refer to the two phases of GRB 911118 and the horizontal dotted line is the slope of the reference spectrum.

of errors in dividing the observed spectrum by the template spectrum. This significance is increased if the first 8 spectra are rebinned in time (although the time resolved information is lost) obtaining a value of $\delta > 0$ at 3.7σ . Anyway, as will be described below for the spectral index global significance, also in the case of GRB 980306 the significance of $\delta > 0$ (Fig. 7) is higher when considering the sequence of δ values as a group (since δ remains systematically positive).

As a final consideration let us stress that in the case of GRB 911118 (Fig. 4) and GRB 980306 (Fig. 3) there is a minority of hard spectra (9 and 4, respectively) which have $\alpha > 0$ at a level of significance lower than 3σ . Nonetheless the fact that a considerable number of subsequent spectra (32 for GRB 911118 and 12 for GRB 980306) in the first few seconds have a spectrum harder (at more than 3σ) than E^0 increases the level of significance of this result, if they are considered as a whole.

4.4. Other hard bursts

There are other bursts with low energy hard spectra for a major part of their evolution, which have already been reported in the literature. In particular, we found three bursts with very hard spectra if fitted by the BAND function. In order to have homogeneous results we have then re-analysed their spectra and also applied the tests described in the previous subsection. Let us summarise their properties.

- GRB 910807 is a weak burst with a peak flux of (7.2 ± 0.5) phot $\text{cm}^{-2} \text{ s}^{-1}$. The spectrum is harder than $\alpha = 0$ for the first ~ 5 s, and remains quite constant (~ 0) during the overall burst, which lasts about 28 s, as already pointed

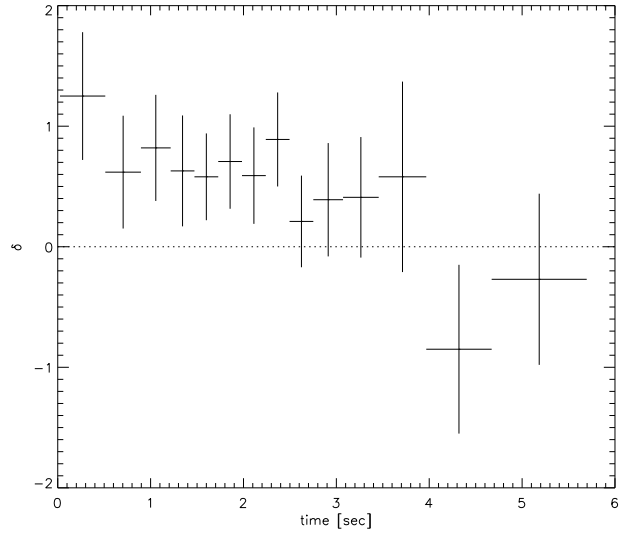


Fig. 7. As Fig. 6 for GRB 980306.

out by Ryde et al. (1999). The peak energy instead shows a tracking pattern correlated with the flux and hardens in correspondence of the second peak (at $t = 12$ s).

The complete spectral evolution is reported in Fig. 8. The hardest spectrum has $\alpha = 1.6 \pm 0.5$ at 90% confidence level. This value is somewhat harder, but consistent with what quoted by Crider et al. (2000). A (successful) check for the hardness of the first few spectra of this burst has been performed using the last method described in the previous section.

- GRB 910927 (Crider et al. 2000, 1997) and GRB 970111 (Crider et al. 1997; Frontera et al. 2000) are other two cases of extremely hard spectra with a low energy power law spectral index as high as $\alpha = 1.6 \pm 0.3$. GRB 970111 was studied (Frontera et al. 2000) also including the WFC-BeppoSAX data. Its extremely hard low energy spectrum was confirmed to extend down to 5 keV. Unfortunately, the lack of spectral resolution of the GRBM instrument above 40 keV does not allow to study the complete spectrum, especially at its peak.

In addition we found in the spectral catalogue of Preece et al. (2000) other 3 bursts (BATSE triggers 1974, 2855 and 6350) with $\alpha > 0$, but at a low significance level ($< 1\sigma$) and for a short interval of the light curve. Note that also these cases contribute to the $\alpha > 0$ tail of the spectral index distribution reported in Fig. 1.

4.5. Black body spectra

As anticipated we performed fits on the hardest spectra also with a black body shape also to test if the emission is consistent with a thermal model. In fact, the first spectra of all the bursts discussed in this work are typically harder than $\alpha = 0.5$ and thus could be consistent with the Rayleigh-Jeans part of the black body. Note that the fit could however be unacceptable in

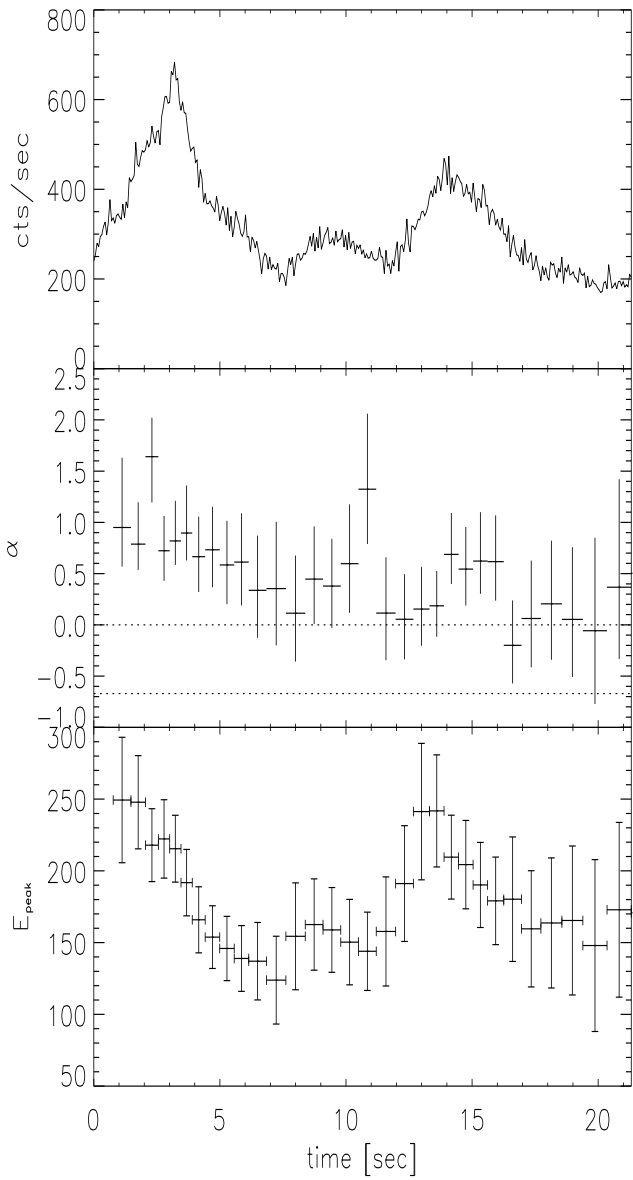


Fig. 8. GRB 910807 spectral evolution. Same as Fig. 3

terms of χ^2 if the curvature around the peak (i.e. typically in the range 100 - 300 keV) were broader than a black body one.

As already mentioned the fits have been performed only on spectra with $\alpha \gtrsim 0.5$ and the criteria applied for the goodness of the fit were

- the reduced χ^2_r should be smaller than a fixed reference value of 1.5. We performed the fits also on spectra with a low energy component softer than our threshold value $\alpha = 0.5$ and found that these fits are unacceptable and typically have $\chi^2_r > 1.5$.
- the model-to-data point ratio can only be systematically and significantly greater than 1 at energies above the peak as a possible consequence of the presence of a supra-

thermal or multi-temperature spectral component whose nature is not discussed here.

The results of the fits are reported in Tab. 2: the start and stop time of each spectrum, with respect to the trigger time, are given in col. 2 and 3. The model temperature kT (keV) and its normalisation ($\text{erg cm}^{-2} \text{ s}^{-1}$) are reported in col. 4 and 5. The value of the reduced χ^2_r and the photon flux computed from the fitted model in the 28–1800 keV energy range are given in col. 6 and 7, respectively. Column 8 and 9 report the spectral index (α) obtained by the fit with the non thermal (BAND or COMP) models and the associated χ^2_r .

For illustration, we report in Fig. 9 some examples of fitted spectra for GRB 980306 and the corresponding data-to-model ratio. The first two spectra are considered well fitted by the model because $\chi^2_r = 1.19$ and 0.9, respectively, and the ratio is systematically greater than 1 only at high energies. In the other two cases the black body fits give less acceptable results because the data-to-model ratio shows systematic deviations from 1 at low energies.

In most of the bursts the best fits with the black body model are obtained at the beginning: in the later stages (e.g. after the first 2.5 s in the case of GRB 980306) the low energy component softens as the reduced χ^2 and the model-to-data ratio indicate.

Note that black bodies with temperatures smaller than ~ 30 keV have a limited Rayleigh–Jeans part in the BATSE energy range. Since black body fits in this case are not well determined we have chosen not to consider them as acceptable fits.

The black body temperature and total flux (as derived by the model) evolve in time as reported in Fig. 10 for all the good black body spectral fits. Note the decrease of the temperature with time in almost all these bursts, which in the figure are compared with a dependence $T_{BB} \propto t^{-1/4}$. Although the temperature decreases, the flux slightly increases or remains constant in the first phases, and rapidly decreases thereafter.

Although not publicly available, it has been reported in poster proceedings of other possible evidences of a black body emission from GRBs (Palmer D. *private communication*).

5. Discussion

GRB 980306 and 911118, together with GRB910807, 910927 and 970111 present in the literature, bring new constraints on the extremely hard spectra that the emission process responsible for the prompt phase must be able to satisfy. For the bursts studied here α , i.e. the spectral index of the low energy photon spectrum, remains positive for a major part of the pulse/s, like in the case of GRB 911118 or GRB 970111, or for its first rising part (GRB 980306 and GRB 910807). These results extend the α distribution reported by Preece et al. (2000) and Ghirlanda, Celotti & Ghisellini al. (2002) to values greater than 0, up to $\alpha \sim 1.5$.

In the following we consider several emission models proposed so far to see if they can account for these hard spectra and in particular we discuss in Sec. 5.7 the quasi-thermal character of the initial phases of these extremely hard bursts.

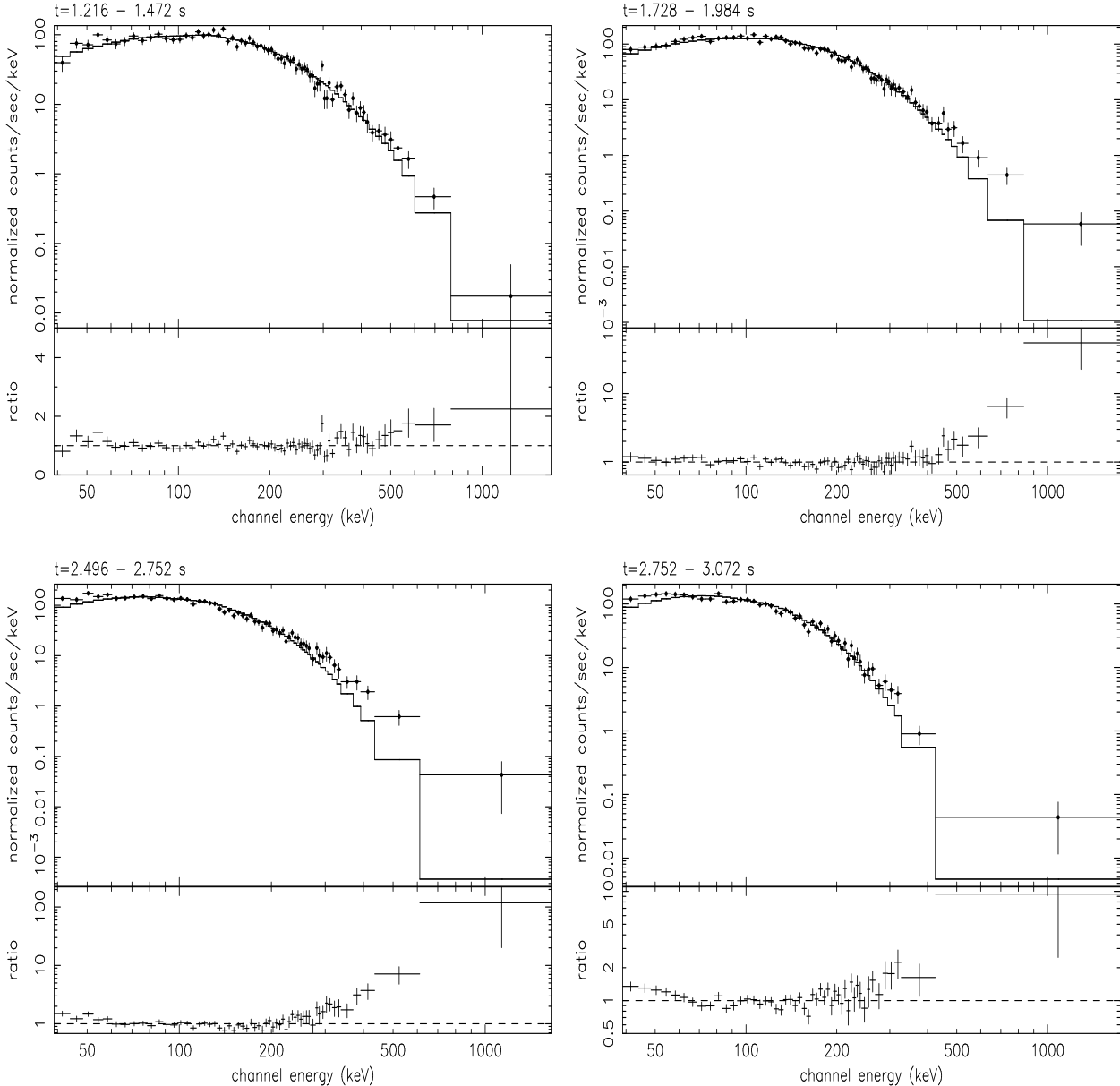


Fig. 9. Examples of black body fits for GRB 980306 (see Tab.2). The integration times are indicated for each plot. The data-to-model ratio are reported in the bottom panels.

5.1. Synchrotron emission

Standard thin synchrotron emission — The thin synchrotron model, in its simplest formulation, can produce at most a spectrum as hard as $\alpha = -2/3$ (Katz 1994). Furthermore if one considers the very short cooling timescales (much shorter than any conceivable current exposure time) the predicted ‘cooled’ spectrum has $\alpha = -3/2$ (Ghisellini, Celotti & Lazzati 2000).

Synchrotron self-absorption — One alternative, investigated among others by Papathanassiou (1999), is that the medium responsible for the synchrotron emission also absorbs these photons.

In this case it is possible to produce low energy spectral slopes as hard as $\alpha = 1$ (for a thermal or a power law electron energy distribution with a low energy cut-off) or $\alpha = 1.5$ (for a power law extending to low energies).

However, for synchrotron self-absorption to be effective in the typical BATSE energy range, a very high density of relativistic electrons is necessary. Assuming that the electron distribution extends to low energies (this minimises the required particle number) with a power law distribution of index p (i.e. $N_e(\gamma) \propto \gamma^{-p}$, where γ is the Lorentz factor of the electrons), the synchrotron self-absorption frequency ν_t in the comoving

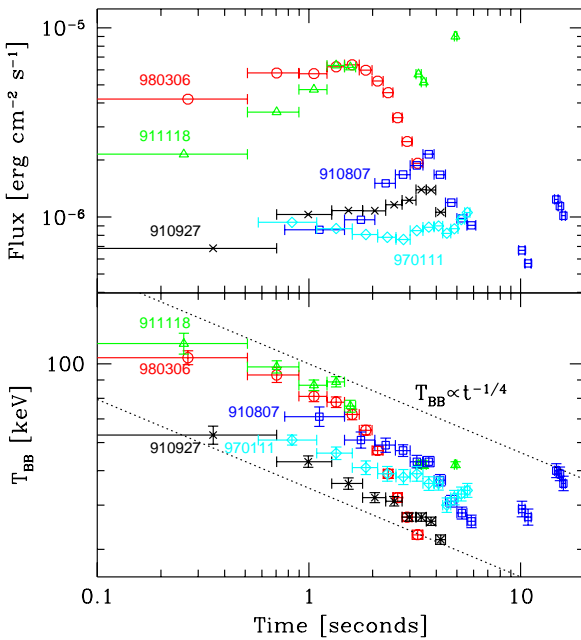


Fig. 10. Total flux (top panel) and black body temperature (bottom panel) as a function of time for the spectra reported in Tab. 2 and considered acceptable in terms of residuals. The dashed lines in the bottom panel correspond to $T_{BB} \propto t^{-1/4}$.

frame, assuming an energy spectral index $p = 2$ for the electrons, is (e.g. Ghisellini & Svensson 1991)

$$\nu_t \simeq 2 \times 10^5 \nu_B (\tau_T/B)^{1/3} \text{ Hz}, \quad (1)$$

where τ_T is the Thomson optical depth, $\nu_B = eB/(2\pi m_e c)$ is the Larmor frequency. In order to have $\nu_t \sim 10^{16}$ Hz, corresponding to $\sim \Gamma \nu_t$ in the BATSE range, we need $\tau_T B^2 \sim 5.7 \times 10^{12} \nu_{t,16}^3$. The Comptonization parameter $y \sim \tau_T \langle \gamma^2 \rangle$, for the required particle density, would largely exceed unity (making inverse Compton process more efficient than synchrotron) unless the optical depth is $\tau_T \sim 1$. This would imply (by eq.(1)) an extremely high magnetic field $B \sim 2 \times 10^6$ G.

Synchrotron from a stratified region — Granot, Piran & Sari (2000) have pointed out that if the electrons producing synchrotron emission are accelerated in a shock, than the emission region is plausibly stratified, with the most energetic electrons present only in the vicinity of the shock front, while colder electrons propagate further away from it. This inhomogeneity introduces some modification in the predicted self-absorbed synchrotron spectrum which may be relevant for the interpretation of the afterglow emission, but does not change the above conclusion on the role of synchrotron self-absorption as responsible for the hard γ -ray spectra.

Small pitch angles — Lloyd & Petrosian (2000) have proposed that in the rarefied, highly magnetised plasmas of GRBs turbulence can give origin to an anisotropic pitch angle distribution of emitting particles. In this case the thin synchrotron emission is modified at low energies (compared to the standard

$F(E) \propto E^{1/3}$), with a limiting slope $F(E) \propto E$. This can accommodate some, but not all, of the hard spectra found. Note also that according to this scenario to prevent strong cooling the particles have to be reaccelerated, contrary to one of the basic assumptions of the internal shock scenario, and in order not to be re-isotropized by scattering, the inverse Compton process must be much less efficient than the synchrotron one.

5.2. Jitter radiation

A variant of the standard synchrotron theory, the jitter radiation (Medvedev 2001), can justify flat to mildly inverted low energy spectral slopes. It originates as the emission of relativistic electrons in a non uniform magnetic field: if the inhomogeneity length scale is smaller than the Larmor gyro-radius, the electron jitters around its average direction of motion. Medvedev (2001) proposed a composite model for GRB spectra by assuming the presence of a small scale magnetic field, which causes the jitter radiation component, and a larger scale field producing a standard synchrotron spectrum. The composite spectrum has a broad bump in correspondence of the jitter radiation characteristic energy, which depends only on the magnetic field properties and not on the electron energy and if the small scale field prevails, the spectrum has a limiting low energy spectral index $\alpha = 0$. This implies that only a minority of the hard spectra reported here could be consistent with such a model.

5.3. Compton attenuation

Compton attenuation (Brainerd et al. 1998) can produce a low energy (20–100 keV) hard component because of the propagation and scattering of the intrinsic spectrum by material (not participating to the bulk flow) located between the fireball and the observer. The original high energy spectral shape can be unaltered because of the decline of the Klein–Nishina cross section with energy, while at lower energies, where the scattering process is more efficient, the spectrum is hardened. The most appealing features of this model are that it naturally explains the clustering of the peak energy of bursts around some hundred keV and produces a flat slope at low energies. But in order for this to work, the Thomson optical depth of the scattering material must be quite large (of the order of $\tau_T \sim 10$) and this would smooth out the observed burst light curve by smearing the variability on the smallest time scales. Furthermore, by decreasing the transmitted (spectrally unaltered) flux, this mechanism requires intrinsic powers greater than what we observe, exacerbating the energy budget problem.

5.4. Quasi-thermal Comptonization

The above models are based on the assumption that the emitting particles are highly relativistic, as a result of “instantaneous” acceleration at a shock front. However, if the heating mechanism operates on timescales of the order of the dynamical time (or the light crossing time of a shell in the internal shock scenario), then the heating and cooling processes could balance,

leading to typical energies of the electrons that are sub or only mildly relativistic (Ghisellini & Celotti 1999). In this case the dominant radiation process is Comptonization of seed soft photons by a quasi-thermal particle distribution.

Different models assume different sources for the seed photons and different parameters (i.e. typical size for the emitting region, magnetic field, role of the photospheric radiation, and so on) within the internal shock scenario.

Liang et al. (1997), among the first to propose such process for the prompt emission, considered a relatively large emitting region embedded in a relatively weak magnetic field. This model was applied to GRB 990123 by Liang (1999), who found quite extreme best fit values for the required total power and total number of emitting particles. Ghisellini & Celotti (1999) proposed the Comptonization model on the self-absorbed cyclo-synchrotron radiation produced by the same quasi-thermal particles responsible for the multiple scattering process, and pointed out the role that electron-positron pairs can have in keeping the temperature (or the mean energy) of the particles within a narrow range. On the same line Meszaros & Rees (2000) pointed out the importance of the residual photospheric emission as source of soft photons.

The basic features of the Comptonization model is that, in the quasi-saturated regime a Wien peak with its characteristic $F(E) \propto E^3$ shape can form at high energies (i.e. for $h\nu \sim kT$). In principle this can thus explain very hard spectra. One possible difficulty of this model is the slope at lower energies, whose saturated value should be $\alpha = -1$. A requirement of Comptonization models is that the energy of the seed photons should be of the order of 1-10 keV for $\Gamma \sim 100 - 1000$, in order to produce the observed spectrum. However, if pair formation occurs steady state studies (assuming Maxwellian distributions and pair balance) indicate somewhat larger values of the typical temperatures (of the order of 50 keV, see e.g. Svensson 1982, 1984). Further studies are necessary to understand the role of a non thermal tail to the Maxwellian particle distribution (which may help in decreasing the equilibrium temperature by increasing the pair production rate, see Stern 1999), and to relax the steady state assumption.

5.5. Photospheric emission

When the fireball is becoming optically thin, during the acceleration or coasting phase, its internal energy is emitted with a black body spectrum whose observed temperature is blue-shifted by a factor Γ with respect to the comoving one. Recently, Daigne & Mochkovitch (2002) have explored this possibility, finding quite tight limits on the model of hot fireballs accelerated through internal radiation pressure, imposed by the absence of an initial emission phase (or precursor) with a black body shape. Since we do find that the emission can be modelled by a black body during the first phase, we will explore and discuss this possibility in somewhat more details below (Sec. 6.7.1).

5.6. Compton drag

If the circum-burst environment is characterised by quite a large photon density, as is the case of bursts following a supernova explosion, or for fireballs produced in the matter-evacuated funnel of an hypernova, then there can be a strong interaction between these seed photons and the fireball itself, as postulated in the so-called Compton drag model. The ambient photon energy is boosted by the factor Γ^2 at the expense of the fireball kinetic energy (Lazzati et al. 2000). If the funnel or the young supernova remnant are characterised by a single temperature T_{SN} , and if the fireball does not decelerate, then the emitted spectrum is a black body at a temperature $T \sim \Gamma^2 T_{\text{SN}}$. If instead the seed photons have a range of temperatures (as likely to be in the case of a funnel, hotter in the central parts), and/or the process is so efficient to decelerate the fireball, than the final spectrum will be a superposition of the locally produced black body spectra, as calculated by Ghisellini et al. (2000). The resulting spectrum can indeed resemble the very hard spectra found, at least for the initial part of the burst. In fact, once the first shells have swept up the seed photons, the efficiency of Compton drag is greatly reduced, since the time to replenish the circum-burst environment with seed photons is typically longer than the duration of the burst itself. On the other hand the Compton drag model favours the formation of internal shocks, since after the first shells deceleration, the subsequent ejecta can more easily collide with them and produce shocks. Then another radiation source can become efficient after the first phase (lasting ~ 1 to a few seconds). This possibly also explains the hard to soft evolution: at first the spectrum, due to Compton drag, is very hard at low energies ($F(E) \propto E^2$), whereas at later times the spectrum produced in internal shocks through other processes becomes softer ($F(E) \propto E^{1/3}$ or $\propto E^0$).

5.7. The possible thermal character of the initial phase

The first 1–5 s of the emission of the bursts presented in this work were found to be consistent with a black body spectrum with typical temperatures initially around ~ 100 keV and decreasing to 30–40 keV. After this initial phase a softer (non-thermal or multi-temperature) character of the spectrum becomes dominant. Clearly this behavior can be a powerful diagnostic. In particular it seems to favour two among the proposed models, namely photospheric and Compton drag emission, which both predict – as recalled in Sec. 5.5, 5.6 – a thermal spectrum during the first phases. Here we briefly discuss which physical constraints can be quantitatively gathered from the data.

5.7.1. Photospheric emission

In this scenario we have two options: we can relate the initial phase to a single fireball, in the process of becoming optically thin, or – following Daigne & Mochkovitch (2002) – to an en-

semble of \mathcal{N} shells, (each becoming optically thin at approximately the same distance). In both cases at transparency:

$$\tau_T = \frac{E_f \sigma_T}{2\pi\theta^2 R_t^2 m_p c^2 \Gamma \mathcal{N}} \sim 1, \quad (2)$$

where R_t is the transparency radius of the fireball, collimated into two cones of semi-aperture angle θ , and E_f is the total fireball energy (a fraction ϵ_γ of which is radiated as photons). Assuming that the surface of the fireball is emitting, at R_t , as a black body with a comoving temperature $T' = T_{\text{obs}}/\Gamma$, we have

$$\langle L_{\text{BB}} \rangle = \frac{\epsilon_\gamma E_f}{t_{\text{BB}}} = 2\pi\theta^2 R_t^2 \sigma \left(\frac{T_{\text{obs}}}{\Gamma} \right)^4 \Gamma^2, \quad (3)$$

where $\langle L_{\text{BB}} \rangle$ is the average black body luminosity observed for the time t_{BB} . Both eq. (2) and (3) show a $E_f \propto \theta^2 R_t^2$ dependence, allowing to solve for the bulk Lorentz factor:

$$\begin{aligned} \Gamma &= \left(\frac{\sigma_T \sigma}{m_p c^2} \frac{T_{\text{obs}}^4 t_{\text{BB}}}{\epsilon_\gamma \mathcal{N}} \right)^{1/3} \\ &\sim 3 \times 10^3 T_{\text{obs},9}^{4/3} t_{\text{BB}}^{1/3} \epsilon_\gamma^{-1/3} \mathcal{N}^{-1/3} \end{aligned} \quad (4)$$

with $T_{\text{obs}} = 10^9 T_{\text{obs},9}$ K. We stress that this estimate of Γ is independent of the degree of collimation of the fireball.

In the case of a single shell t_{BB} is the time needed for the fireball to become transparent, implying

$$R_t = ct_{\text{BB}} \Gamma^2 \sim 3 \times 10^{17} T_{\text{obs},9}^{8/3} t_{\text{BB}}^{5/3} \epsilon_\gamma^{-2/3} \text{ cm}. \quad (5)$$

Therefore, if the emission comes from a single shell, the transparency radius is very large, and this implies unreasonably large values for the luminosity and energy. In fact, substituting the values for Γ and R_t into eq.(3) we have

$$E_f \sim 3 \times 10^{58} \theta_{-1}^2 T_{\text{obs},9}^{20/3} t_{\text{BB}}^{11/3} \epsilon_\gamma^{-5/3} \text{ erg}. \quad (6)$$

where θ is expressed in units of 0.1 radians.

If, instead, the observed emission comes from a series of shells the transparency radius can be much smaller, allowing a “reasonable” luminosity of the photosphere: for $E_f = 10^{51} E_{f,51}$ erg we have

$$R_t \sim 5 \times 10^{13} \frac{E_{f,51}^{1/2}}{\theta_{-1} \mathcal{N}^{1/3}} \left(\frac{\epsilon_\gamma}{t_{\text{BB}} T_{\text{obs},9}^4} \right)^{1/6} \text{ cm}. \quad (7)$$

We conclude that a series of shells (of total energy E_f) each becoming transparent at R_t can account for the observed black body emission. The case of \mathcal{N} shells for large \mathcal{N} is clearly equivalent to a continuous or quasi-continuous flow.

As Daigne & Mochkovitch (2002) pointed out, the photospheric radiation is likely to be visible only during the first phases of the burst light curve, as long as the optical depth of the material ahead of the shell which is releasing its thermal radiation is negligible and before internal shocks take over.

5.7.2. Compton drag

We assume that the time interval for which the black body lasts corresponds to the emission from a single shell (since as mentioned above we have difficulties in explaining how to replenish the circum-burst environment with seed photons for the subsequent shells). We also assume that the emission peaks when the shell becomes transparent (eq. 2), implying $R_t \sim ct_t \Gamma^2$.

In general, the observed temperature is a factor $\sim 2\Gamma^2$ larger than the temperature of the seed photons T_{NS} . The total energy E_{CD} due to the Compton drag process, produced in the observed time t_t , is of the order

$$\begin{aligned} E_{\text{CD}} &\sim 2\pi\theta^2 R_t^3 (2\Gamma^2) a \left(\frac{T_{\text{obs}}}{2\Gamma^2} \right)^4 \\ &\sim 3 \times 10^{51} \theta_{-1}^2 t_t^3 T_{\text{obs},9}^4 \text{ erg}. \end{aligned} \quad (8)$$

In this form E_{CD} does not depend on Γ (although of course T_{NS} does). We can then derive the transparency radius (from eq.(2) and (8)) and the bulk Lorentz factor:

$$\begin{aligned} R_t &= \left(\frac{\sigma_T c^{3/2} t_t^{7/2} a T_{\text{obs}}^4}{8\epsilon_\gamma m_p} \right)^{2/5} \\ &\sim 3 \times 10^{14} T_{\text{obs},9}^{8/5} t_t^{7/5} \epsilon_\gamma^{-2/5} \text{ cm} \end{aligned} \quad (9)$$

$$\Gamma = \left(\frac{R_t}{ct_t} \right)^{1/2} \sim 100 T_{\text{obs},9}^{4/5} t_t^{1/5} \epsilon_\gamma^{-1/5} \quad (10)$$

for a temperature of the seed photons corresponding to $T_{SN} \sim 5 \times 10^4$ K.

These simple (and rough) estimates indicate that the Compton drag model is viable.

5.7.3. Time evolution

Although the limited number of time resolved spectra and bursts do not allow to search for a general evolutionary behaviour, we can briefly comment on the spectral and dynamical evolution of the initial thermal phase of these 5 bursts. As reported in Fig. 10 in all the 5 bursts, the black body temperature (T_{obs}) decreases with time (bottom panel) and its evolution is intriguingly close to $T_{\text{obs}} \propto t^{-1/4}$ for the first few seconds, and then drops. In the same time interval the luminosity (L_{BB}) remains constant or mildly increases (top panel of Fig. 10). We therefore observe, at least in the first phase, a decrease in the observed temperature without a corresponding decrease in the observed black body flux.

We plan to examine more deeply these observational facts in a future work: here we would like only to mention some generic possibilities.

In the context of the photospheric model discussed in Sec. 5.7.1, the blackbody evolution could be explained by successive shells having an increasing baryon loading and smaller Lorentz factor, thus becoming transparent at increasing distances R_t . This can cause the observed temperature to decrease (because the Lorentz factor is smaller) without a decrease in flux (because the radius is larger).

In the context of the Compton drag model, a decrease in the observed temperature can be due to the deceleration of the fireball and/or a decreasing (with distance) temperature of the seed photons. If we consider the luminosity due to the Compton drag process (Eq. (8)), we have $L_{\text{CD}} \propto E_{\text{CD}}/t \propto t^2 T_{\text{obs}}^4$, which predicts $L_{\text{CD}} \propto t$ if the time behavior of the observed temperature is indeed $T_{\text{obs}} \propto t^{-1/4}$. A weaker dependence of the observed flux on time can occur if the fireball is becoming transparent (i.e. only a fraction τ_T of the seed photons can be scattered) with τ_T decreasing with distance and/or if the fireball

distance becomes larger than the typical dimension occupied by the seed photons.

6. Conclusions

In this work we have presented the spectral evolution of GRB 911118 and of a new case of hard burst, GRB 980306, together with some other hard bursts already reported in the literature. Their low energy spectral component is harder than $N(E) \propto E^0$ for a considerable period of their main peak emission and even after this initial phase their spectrum remains harder than the synchrotron limit $E^{-2/3}$. We have applied different tests to verify the significance of the low energy hardness, concluding that these results are indeed robust.

These GRB prompt spectra represent a challenge for the proposed emission scenarios as shown through a comparison with the limiting spectral shapes predicted by such models. We pointed out the difficulties that synchrotron emission, even including the effects of self-absorption, small pitch angles particle distributions and jittering, has in explaining spectra harder than $N(E) \propto E^0$. Comptonization models also have difficulties, even if their are consistent with very hard spectra in a limited range of energies.

The main new result of this study is the possible thermal character of the first emission phase of all the bursts we considered. The conventional scenario, of a fireball accelerated by its own internal pressure, indeed *predicts* such an initial thermal character when the fireball becomes transparent. It was indeed its absence in previously considered bursts that led Daigne & Mochkovitch (2002) to favour a rather cold fireball scenario, where at least part of the acceleration was due to magnetic forces. In our bursts, on the contrary, the luminosity in the thermal phase is a significant fraction of the total, therefore in agreement with the hot fireball scenario. However, the fireball could be cold initially, and be heated later (but before it becomes transparent). The heating agent could be magnetic reconnection (see e.g. Drenkhahn & Spruit 2002) or internal shocks occurring at early phases. The latter case demands that the typical bulk Lorentz factors of the shells are small enough for the shells to collide before the transparency radius.

Alternatively, a cold fireball could work if the thermal spectrum we see is produced by Compton drag, in which circum-burst radiation is boosted to high energies by the fireball bulk motion.

At present, we are not able to discriminate between the photospheric and the Compton drag scenario. Consider also that emission at times greater than a few seconds can well be due to other processes, possibly linked to internal shocks starting to dominate at later phases. However, a key difference between the two scenarios is the fact that the seeds photons for the Compton drag process can be “used” only by the first shells, because the time needed to refill the scattering zone with new seeds exceeds the duration of the burst. Therefore observing blackbody emission for a long time, or during the rising phase of two time resolved peaks would be difficult to explain in terms of the Compton drag process.

Acknowledgements. This research has made use of data obtained through the High Energy Astrophysics Science Archive Research Center Online Service, provided by the NASA/Goddard Space Flight Center. Giancarlo Ghirlanda and AC acknowledge the Italian MIUR for financial support.

References

Amati L., Frontera F., Costa E., et al., 1999, A&AS, 138, 403
 Band D.L., Matteson J.L. & Ford L.A., 1993, ApJ, 413, 281
 Bevington P. R. & Robinson D. K. *Data reduction and error analysis for the physical science*, McGraw-Hill 1992 2nd ed.
 Böttcher M., Dermer C.D., Crider A.W. & Liang E.P., 1999, A&A, 343, 111
 Brainerd J.J., 1994, ApJ, 428, 21
 Brainerd J.J., Preece R.D., Briggs M.S., Pendleton G.N. & Paciesas, W.S., 1998, ApJ, 501, 325
 Crider A., Liang E.P., Smith I.A., 1997, ApJ, 479, L39
 Crider A., Liang E.P. & Preece R.D., 1997, astro-ph/9711100
 Crider A. & Liang E.P., 1999, ApJ, 519, 206
 Crider A. & Liang E.P., 2000, ApJ, 127, 283
 Crider A. & Liang E.P., 1999, A&AS, 138, 405
 Daigne F. & Mochkovitch R., 2002, MNRAS, in press (astro-ph/0207456)
 Dermer C. & Böttcher M., 2000, ApJ, 534, L155
 Ford L. A *Guide to Spectroscopic Oriented Routines*, v. 1.2, 1993
 Ford L.A., Band D.L. & Matteson J.L., 1995, ApJ, 439, 307
 Drenkhahn G. & Spruit H.C., 2002, A&A, 391, 1141
 Frontera F., Amati L., Costa E., et al., 2000, ApJS, 127, 59
 Ghirlanda G., Celotti A. & Ghisellini G., 2002, A&A, in press
 Ghisellini G., Lazzati D., Celotti A. & Rees M.J., 2000, MNRAS, 316, L45
 Ghisellini G. & Celotti A., 1999, ApJ, 511, L93
 Ghisellini G. & Svensson R., 1991, MNRAS 252, 313
 Granot J., Piran T. & Sari R., 2000, ApJ, 534, L163
 Katz J.I., 1994, ApJ 432, L107
 Lazzati D., Ghisellini G., Celotti A. & Rees M.J., 2000, ApJ, 529, L17
 Lloyd N.M. & Petrosian V., 2000, ApJ, 543, 722
 Lloyd N.M. & Petrosian V., 2002, ApJ, 565, 182
 Liang E., Kusunose M., Smith I.A. & Crider A., 1997, ApJ, 479, L35
 Liang E., 1999, A&AS, 138, 529
 Medvedev M.V., 2001, astro-ph/0001314
 Meszaros P. & Rees M.J., 2000, ApJ, 530, 292
 Panaiteescu A. & Meszaros P., 2000, ApJ, 544, L17
 Papathanassiou H., 1999, A&AS, 138, 525
 Preece R.D., Pendleton G.N. & Briggs M.S., 1998, ApJ, 496, 849
 Preece R.D., Briggs M.S. & Mallozzi R.S., 2000, ApJS, 126, 19
 Preece R.D., Briggs M.S., Mallozzi R.S., Pendleton G.N., Paciesas W.S. & Band D.L., 1998, ApJ, 506, L23
 Rees M.J. & Meszaros P., 1994, ApJ, 430, L93
 Ryde F. & Svensson R., 1999, ApJ, 512, 693
 Stern B., 1999, in *High Energy Processes in Accreting Black Holes*, eds. J. Poutanen and R. Svensson, ASP Conf. Series, Vol. 161, p. 277 (astro-ph/9902203)
 Svensson R., 1982, ApJ, 258, 321
 Svensson R., 1984, MNRAS, 227, 403
 Tavani M., 1996, ApJ, 466, 768

Table 2. Black body fits.

GRB	t_{start} sec	t_{stop} sec	kT keV	N erg/cm ² sec	χ^2_{red}	F phot/cm ² sec	α	$\chi^2_{\text{red}, \alpha}$
980306	0.024	0.512	$104^{+4.8}_{-4.8}$	$46^{+2.7}_{-2.8}$	1.15	8.4	0.86 ± 0.15	1.09
	0.512	0.896	$93^{+4.6}_{-3.9}$	$63^{+3.8}_{-2.8}$	1.27	12.9	0.98 ± 0.13	1.21
	0.896	1.216	$81^{+2.8}_{-2.9}$	$63^{+2.8}_{-2.8}$	1.27	14.7	1.01 ± 0.13	1.2
	1.216	1.472	$78^{+2.7}_{-2.6}$	$68^{+3.1}_{-3.0}$	1.19	16.6	1.11 ± 0.14	1.19
	1.472	1.728	$72^{+2.5}_{-2.5}$	$70^{+3.1}_{-3.0}$	1.44	18.4	0.61 ± 0.12	1.12
	1.728	1.984	$65^{+2.1}_{-2.1}$	$66^{+2.7}_{-2.6}$	0.86	19.10	0.73 ± 0.12	0.7
	1.984	2.24	$57^{+1.6}_{-1.8}$	$59^{+1.7}_{-2.6}$	1.33	19.09	0.8 ± 0.13	1.16
	2.24	2.496	$49^{+1.5}_{-1.4}$	$52^{+1.8}_{-1.8}$	1.26	19.3	0.61 ± 0.13	0.96
	2.496	2.752	$42^{+1.3}_{-1.4}$	$39^{+1.3}_{-1.4}$	1.39	16.6	0.19 ± 0.14	0.8
	2.752	3.072	$37^{+1.1}_{-1.1}$	$30^{+0.9}_{-0.9}$	1.45	14.1	0.56 ± 0.17	1.2
911118	3.072	3.456	$33^{+1.0}_{-1.0}$	$23^{+0.7}_{-0.8}$	1.23	12.14	0.52 ± 0.19	1.0
	0.000	0.512	$114^{+8.0}_{-8.0}$	$23^{+2.0}_{-3.0}$	0.95	3.92	0.71 ± 0.24	0.8
	0.512	0.896	$98^{+4.0}_{-5.0}$	$39^{+2.0}_{-3.0}$	1.39	7.61	0.55 ± 0.12	1.1
	0.896	1.216	$87^{+3.0}_{-5.0}$	$52^{+3.0}_{-3.0}$	1.51	11.28	0.59 ± 0.11	1.2
	1.216	1.472	$89^{+3.0}_{-4.0}$	$69^{+4.0}_{-4.0}$	1.45	14.78	0.51 ± 0.11	1.0
	1.472	1.664	$76^{+3.0}_{-3.0}$	$68^{+4.0}_{-3.0}$	1.35	16.93	0.74 ± 0.13	1.1
	3.2	3.392	$52^{+1.0}_{-1.0}$	$65^{+2.0}_{-2.0}$	1.52	22.76	0.5 ± 0.1	0.9
	3.392	3.584	$52^{+1.3}_{-2.0}$	$59^{+2.0}_{-2.0}$	1.51	20.61	0.57 ± 0.1	0.87
910807	0.768	1.472	$71^{+4.6}_{-4.6}$	$9.4^{+0.8}_{-0.8}$	1.10	2.51	0.95 ± 0.29	1.2
	1.472	2.048	$61^{+3.3}_{-3.3}$	$11^{+0.9}_{-0.9}$	1.29	3.3	0.78 ± 0.21	1.0
	2.048	2.56	$59^{+2.8}_{-2.6}$	$17^{+0.8}_{-0.8}$	1.05	5.32	1.64 ± 0.25	0.8
	2.56	3.008	$57^{+2.2}_{-2.3}$	$19^{+1.2}_{-2.3}$	0.78	6.12	0.72 ± 0.19	0.84
	3.008	3.456	$53^{+2.2}_{-2.1}$	$21^{+0.9}_{-0.9}$	0.94	7.36	0.82 ± 0.18	0.95
	3.456	3.904	$53^{+1.8}_{-1.9}$	$24^{+1.0}_{-1.0}$	1.00	8.43	0.89 ± 0.21	1.06
	3.904	4.416	$47^{+1.8}_{-1.7}$	$19^{+0.8}_{-0.8}$	1.09	7.42	0.67 ± 0.23	0.97
	4.416	4.992	$41^{+1.6}_{-1.6}$	$14^{+0.6}_{-0.6}$	1.06	6.05	0.58 ± 0.25	1.0
	4.992	5.568	$38^{+1.5}_{-1.6}$	$11^{+0.5}_{-0.5}$	0.84	5.39	0.61 ± 0.28	1.1
	5.568	6.144	$36^{+1.5}_{-1.5}$	$11^{+0.5}_{-0.5}$	1.11	5.23	0.6 ± 0.33	1.17
	6.144	10.496	$39^{+2.0}_{-1.9}$	$7.7^{+0.4}_{-0.4}$	1.24	3.56	1.32 ± 0.40	1.63
	10.496	11.2	$37^{+2.0}_{-2.0}$	$6.8^{+0.4}_{-0.4}$	1.21	3.2	0.54 ± 0.23	1.03
	14.464	15.04	$50^{+2.3}_{-2.2}$	$14^{+0.7}_{-0.8}$	0.83	5.16	0.62 ± 0.24	0.83
	15.04	15.616	$49^{+2.2}_{-2.2}$	$13^{+0.6}_{-0.7}$	1.11	4.851	0.62 ± 0.27	1.4
	15.616	16.256	$46^{+2.2}_{-2.2}$	$12^{+0.6}_{-0.7}$	0.9	4.6		
910927	0.000	0.704	$63^{+3.8}_{-3.8}$	$7^{+0.6}_{-0.5}$	0.82	2.26	0.62 ± 0.26	0.96
	0.704	1.28	$53^{+3.0}_{-2.4}$	$12^{+0.6}_{-0.6}$	0.91	4.05	1.02 ± 0.28	0.93
	1.28	1.792	$46^{+1.7}_{-1.7}$	$12^{+0.6}_{-0.6}$	1.3	4.9	1.04 ± 0.25	1.13
	1.792	2.304	$42^{+1.4}_{-1.3}$	$12^{+0.5}_{-0.6}$	1.23	5.35	1.24 ± 0.24	0.9
	2.304	2.752	$41^{+1.3}_{-1.4}$	$14^{+0.5}_{-0.6}$	0.99	5.9	1.1 ± 0.24	0.8
	2.752	3.2	$37^{+1.1}_{-1.2}$	$15^{+0.6}_{-0.5}$	0.98	6.9	1.05 ± 0.24	1.0
	3.2	3.584	$37^{+1.0}_{-1.2}$	$17^{+0.5}_{-0.7}$	0.98	7.85	1.12 ± 0.25	1.0
	3.584	3.968	$36^{+1.0}_{-1.0}$	$17^{+0.6}_{-0.6}$	0.99	8.03	0.98 ± 0.19	1.1
	3.968	4.416	$32^{+1.0}_{-1.0}$	$13^{+0.5}_{-0.5}$	0.8	6.9	0.83 ± 0.2	0.8
	4.416							
970111	0.576	1.088	$61^{+2.0}_{-2.0}$	$11^{+0.8}_{-0.8}$	0.97	3.2	1.51 ± 0.4	0.96
	1.088	1.6	$56^{+2.3}_{-2.3}$	$10^{+0.6}_{-0.6}$	1.15	3.23	1.31 ± 0.34	1.07
	1.6	2.112	$51^{+2.3}_{-2.3}$	$9.3^{+0.6}_{-0.6}$	1.00	3.3	1.11 ± 0.28	0.9
	2.112	2.58	$49^{+2.4}_{-2.4}$	$9^{+0.6}_{-0.6}$	1.43	3.32	1.02 ± 0.31	1.2
	2.58	3.008	$48^{+2.4}_{-2.4}$	$9^{+0.6}_{-0.6}$	0.98	3.3	1.6 ± 0.4	0.9
	3.008	3.456	$49^{+2.4}_{-2.4}$	$10^{+0.6}_{-0.6}$	0.93	3.6	1.02 ± 0.32	0.8
	3.456	3.904	$46^{+2.1}_{-2.4}$	$10^{+0.5}_{-0.6}$	0.97	4.0	1.85 ± 0.38	0.7
	3.904	4.288	$46^{+2.0}_{-2.0}$	$10^{+0.6}_{-0.6}$	0.95	4.06	1.83 ± 0.4	0.9
	4.288	4.672	$40^{+1.9}_{-1.4}$	$9.7^{+0.6}_{-0.6}$	1.16	4.27	1.25 ± 0.31	1.2
	4.672	5.056	$42^{+2.0}_{-2.0}$	$10^{+0.6}_{-0.6}$	1.13	4.3	1.34 ± 0.41	0.92
	5.056	5.44	$43^{+2.0}_{-2.0}$	$11^{+0.7}_{-0.7}$	0.96	4.7	0.79 ± 0.31	1.07
	5.44	5.76	$44^{+2.0}_{-2.0}$	$12^{+0.7}_{-0.7}$	0.85	5.0	0.84 ± 0.28	0.82